Digital Manufacturing Technology
https://ojs.wiserpub.com/index.php/DMT/

UNIVERSAL WISER PUBLISHER

Research Article

Sum Standard Deviation of Frequency – A Context Independent Machine Condition Trend Indicator

Shi Feng, John P. T. Mo*

School of Engineering, RMIT University, Melbourne, VIC 3000, Australia
E-mail: john.mo@rmit.edu.au

Received: 20 June 2023; **Revised:** 19 August 2023; **Accepted:** 11 September 2023

Abstract: In Industry 4.0, multiple research subjects have been involved in processing enormous information generated during the manufacturing process. Meanwhile, they all pursue the same goal, that is, to maintain the manufacturing process at good operating state. Hence, many researchers are focusing their researches on continuous health monitoring using digital signal processing techniques, in particular, most researches are focused on recognition of a fault condition only. However, by the time when a fault is recognised, at least one reject has been produced, or an impact to the system's operation has occurred. In addition, many algorithms are designed specifically for certain class of applications. This paper proposes a new system health condition indicator, Sum Standard Deviation of Frequency (SSDF), which is computed from a new computational process that segments raw data streams into time segments and the segments are synchrosqueezed continuous wavelet transformed. As long as sufficient data is available, SSDF shows distinct consecutive regions for "normal", "marginal" and "abnormal" machine conditions. Actions can then be taken while the machine is in "marginal" conditions in which the manufacturing quality is still acceptable. SSDF does not link to any application context information of the raw signal data stream hence making it context independent.

***Keywords*:** fault diagnostics, fault prognostics, synchrosqueezed wavelet transform, scalogram, standard deviation of frequency, SSDF

Nomenclature

$W(a, b; \psi)$	Continuous wavelet transform (CWT) coefficient
$W(a, b)$	CWT coefficient using default mother wavelet
a	Scale parameter of CWT
b	Shaper parameter of CWT
$\psi_{a,b}(t)$	Mother wavelet
$x(t)$	Signal stream
$SG(a, b; \psi)$	Scalogram of CWT
$W_i(a, b; \psi)$	CWT coefficient of segment i
$SG_i(a, b; \psi)$	Scalogram of CWT of segment i
t_T	Total sampled time
n	Number of time segments in a data stream

Copyright ©2023 Shi Feng, et al.
DOI: https://doi.org/10.37256/dmt.3220233254
This is an open-access article distributed under a CC BY license
(Creative Commons Attribution 4.0 International License)
https://creativecommons.org/licenses/by/4.0/

t_0	Data segment overlap time
t_s	Length of time segment
$\omega(a, b)$	Instantaneous frequency at signal point (a, b)
$T(\omega_l, b)$	Syncrhrosqueezed CWT of segment i
ω_l	Synchrosquqeezed CWT boundary parameter
$\Delta\omega$	Synchrosquqeezed CWT width of boundary
$SSG_i(a, b; \psi)$	Synchrosqueezed CWT scalogram
F_{stdf}	Standard deviation of frequency of scalogram
F_{cf}	Centre frequency of scalogram
Z_{stdf}	Sum standard deviation of frequency
Z_{jstdf}	Standard deviation of frequency of jth segment

1. Introduction

Health monitoring has the assumption that the system deteriorates over time so that continuous monitoring of certain operating parameters of the system will be able to detect problems before they occur. Therefore, the ability to continuously measure and process signals from the system to check its status is a prerequisite to health monitoring. With the advancement of Industry 4.0 environment, many data intensive monitoring activities become possible. A good example is monitoring wear and tear on cutting tools. The idea is to monitor certain conditions on the system by some indicative measures based on a theoretical model of the operation so that the decision to stop and repair can be made before the cutting tool malfunctions [1]. The model used temperature, vibration, power consumption as indicators. Sensors were installed on the machine to capture information online.

One of the difficult issues in health monitoring is the prevention of faults. Faults are abrupt deterioration of the machine's capabilities leaving the machine operator almost no time to take remedial action preventing rejects or causing damage to the machine. Detection of faults requires instantaneous machine signal discrimination. German-Sallo and Strnad [2] applied a digital signal processing method to adaptive mode decomposition based procedure to process instantaneous frequency and amplitude as indicators to detect faults in noisy environment successfully.

Wear and tear phenomenon can be hypothesised as loss of materials on surface (wear) in a process of continuous generation of micro-cracks causing materials breaking off bit-by-bit. Wei et al. [3] evaluated micro-cracks on rotary ultrasonic grinding machine. The fractal density of micro-cracks changed as grinding forces were increased. The research found that demonstrated that the occurrence of a crack could be predicted provided that the right evaluation parameter was used. On the same token, a fault can be thought of as the result of accumulation of micro-faults to the point that the system is no longer able to sustain its operation. The problem is how to monitor the accumulation of such micro-faults, whereas in comparison, micro-cracks could be evaluated with some observable characteristics. Long et al. [4] reviewed the application of signal processing of ultra-high frequency signals to partial discharge detection. Three categories of digital processing technologies were used: preprocessing, source localisation and pattern recognition. Effectiveness of digital processing techniques in fault monitoring depends on appropriate processing techniques with relevant indicators.

Kia et al. [5] reviewed a broad range of digital signal processing techniques for the purpose of induction machine fault diagnosis. By analysing the signals in the domains of frequency, time and time-frequency, they concluded that digital signal processing methods could identify the occurrence of faults within a reasonable time if the signals were harmonic. However, engineering systems are becoming more complex. More sophisticated diagnosis methods such as long-short-term memory (LSTM) [6] to detect and classify fault types as multiple sensor signals on rotary machinery drivetrain. Likewise, recurrent neural network (RNN) was used to improve detection of defects that disappeared and exploded easily in a chemical process [7]. It is evident that signal processing is a common diagnosis method among machine systems from which continuous time data stream can be captured. The time domain signals could be analysed by many mathematical transformations and consolidated to one or more indicators. The problem is what indicators can allow such differences to be differentiated from the system in trouble. Incorrect indicators not only waste time but also risk making incorrect decisions, for example, further damaging the system or producing more rejects from the process.

Unfortunately, trend indicators are often system and environment specific. A change in the operating environment

could invalidate the indicator. Pedrosa and Vieira [8] developed a fault locating method using values of voltage deviations in the impedance matrix as the fault indicators. The analysis required a correlation index to be computed and an automatic mapping interruption procedure to mitigate multiple estimation problems. The method identified faulted zones and multiple fault locations correctly. Further research was expected to make the method less dependent on impedance, which was specific to the system. Zhao et al. [9] used remote signaling and telemetering as fault indicators to monitor three phase current in power distribution systems. With the trigger of fault indicators, the time-based wave data were sampled and Fourier transformed to obtain the current phasor, which was used to synchronise errors between fault phase and non-fault phase. Compared with normal signal processing methods, further analysis of the fault indicators is essential to identify the status of the fault. The specificity of fault indicators in these cases makes it difficult for the methods to be generally used in any health monitoring requirements.

This paper proposes a generic process signal indicator that can be applied to all systems universally and in a broad range of machine setup conditions. It is capable of differentiating faults from normal situations. The new processed signal indicator, Sum Standard Deviation of Frequency (SSDF), is the outcome of a novel signal segmentation process plus a series of continuous wavelet transformations and statistical processing. Computation of SSDF is independent of what the system is being monitored. It only requires continuous time-based signals as input and does not depend on any constraint on the system such as location. Early warnings can be raised so that operators can stop the fault accumulation during the manufacturing process, which avoid material waste, workpiece rejects, and cut off the maintenance downtime.

2. Literature review

Fault diagnostic systems require an enormous amount of real-time data to be processed. Common digital signal processing methods such as Fast Fourier Transform [10] and Statistical Process Control [11] have been used in earlier research and industrial applications. With more advanced computational platforms being made available, more sophisticated digital signal processing technologies have been used. Irrespective of changes in the method of data processing, the fundamental principle that some kind of characterising computational values are used in all cases as condition indicators [12]. The following literature review focuses on different types of machine condition indicators, their origin, properties and applications.

2.1 *Frequency domain characterised indicators*

Extending from traditional Fourier Transform methods, the Short-Time Fourier Transform provides more focus fault detection capability. Using Short-Time Fourier Transform techniques, Balamurugan et al. [13] transformed voltage and current waveforms from a photovoltaic electric arc test bed and identified faults in frequency domain. Their frequency-based fault indicators were able to detect fault conditions repeatedly. Ahmadi et al. [14] excited concrete piers of bridge by a small impact load. The time-based signals were processed by Short-Time Fourier Transform to compute a damage index and compared to frequency matrices to find damage locations. To analyse the extent of damage, a finite element model of the bridge was required. However, the methodology has its deficiency because of the window size. Time and frequency resolution at different parts of the signal varies. The accuracy of detection is not guaranteed.

Continuous wavelet transform (CWT) has been a popular signal processing tool since its appearance [15]. CWT has the advantage that the window size can be adjusted. CWT can adjust the shape of its mother wavelet thus filtering unnecessary information from the signal and providing clearer discrimination. The window is called wavelet in CWT, by dilating and translating the mother wavelet [16]. Since the size of the wavelet can be adjusted, during the translation, more flexible time and frequency information should be processed to different fault indicators. Lapins et al. [17] used CWT to monitor volcanic activity. The seismic signals had an extremely broad range of frequencies. With the wavelet window localisation property, the volcanic conditions were indicated by spectral characteristics. They concluded that CWT spectrum was able to capture and distinguish volcanic signals from ambient microseismic noise particularly for very-long-period signals.

However, fault characteristics may not necessarily exhibit in the frequency domain. Lee et al. [18] proposed a fuzzified combined function from wavelet transform, phase-space reconstruction and Euclidean distance to classify

normal and epileptic seizure electroencephalography signals. Initially, 24 features were extracted from the frequency distributions. The final fault indicator contained 4 minimum features and was able to achieve high sensitivity, specificity and accuracy. Hence, literature review shows that spectral-based indicators are good to detect changes in frequency characteristics of the collected signals but they are not always discriminative. Different systems have different set of frequency characteristics limiting identifiable properties in frequency domain-based indicators.

2.2 *Indicator based on scalogram*

Scalogram is an application variant based on CWT spectrum. It is computed from the absolute value of CWT coefficient and reflects the abrupt signal change in the CWT spectrum. Visualisation of scalogram is in a graph showing the density of all frequencies. Narin [19] transformed electroencephalogram signals into 2D-scalogram images via CWT processing. The images were compared to scalogram images from patients of different epileptic seizure conditions. With 5 pre-trained models, the system was able to classify over 90% of cases in preparation for neuro-surgery. The fault indicator is the set of scalogram images of processed CWT spectrum. Feng and Mo [20] computed scalogram images from signals collected on an automatic trampoline manufacturing machine. The condition indicator was developed by counting the number of frequencies in different bands. Some faults were detected while they were evolving. However, the results were not conclusive.

In the traditional CWT scalogram analysis, fault features are detected by CWT of the whole data set and observing the colour changes in the scalograms [21]. The single point rubs in gas turbines were detected from proximitors acceleration signals of rotor displacements. The data were transformed by CWT and post-processed by Digital Fourier Transform. The outcome was then used as the proximity indicator to compare with a computational model of the rotating machine. As the system became unstable, the intensity of the scalogram would be detectable. Likewise, Yesilyurt [22] compared the efficacy of spectrogram and scalogram in gearbox fault detection and concluded that scalogram provided better condition indicating information than spectrogram. Four-time dependent indicators were computed from the scalogram: the instantaneous energy, mean and median frequencies, and bandwidth. These indicators were found useful for detecting localised gear damages from dynamic behaviour of the system.

Instead of directly observing the scalogram, the information behind scalogram can be extracted as features for fault diagnostics such as pitting damage in gears. Detection of minor fatigue crack, pit or chip weakness in gears is difficult as the resulting transient signal could be too weak to be noticeable. Ozturk et al. [23] collected vibration signals from a two-stage industrial gearbox. Minor faults were introduced and the time domain signals were processed by CWT. The spectrum was further processed to generate a scalogram. The fault indicator for gearbox diagnosis was the mean frequency variations. Abnormal (fault) problems were identified by comparing patterns of variations.

Wu et al. [24] processed vibration signals from aeroengines into scalograms. They found that the scalograms exhibited some uniform binary patterns that reflected fundamental properties of aeroengine under test. They divided the time and scale information in the traditional scalogram and extracted the energy, entropy, and contrast information. Three patterns that were affected by rub-impact faults were studied. The image and histograms derived from the scalogram proved to be useful indicators of texture features.

Literature review shows that scalograms are good source of fault indicators for abrupt changes causing larger CWT coefficients and displaying brighter colours visually. Computationally, the brighter colour areas could be detected by area counting. However, research also showed that the coefficients were often spread widely such that demarcation between normal and abrupt changes were not always clear. This problem of blurred warning makes scalogram indicators unsuitable for applications without prior verification.

2.3 *Synchrosqueezed scalogram as indicator*

Although scalogram is convenient to apply, the drawback is apparent: low energy concentration caused poor readability, blurs in the scalogram. To solve the problem, Daubechies et al. [25] proposed synchrosqueezing wavelet transform to improve the readability by retrieving the time-vary amplitudes and the instantaneous frequencies in the signal. Their method combined CWT with a zone reallocation so that more “power” in the signal could be mathematically captured. The resulting scalogram is called synchrosqueezed scalogram. It has more concentrated CWT coefficients and displayed more focused frequency bands.

Thakur et al. [26] further demonstrated that synchrosqueezed scalogram were robust and stable in Gaussian white noise environments. They applied the technique to extract characteristics of paleoclimate change from data over 2.5 million years where the sampled data varied in uniformity and accuracy. Likewise, Mihalec et al. [27] found that analysing damping ratios of a vibrating system using synchrosqueezing technique was not sufficiently accurate. They investigated three different strategies: scale-dependent coefficient, shifted-coefficient and autocorrelated frequency. The improvements performed better than the original synchrosqueezed scalogram.

Gundewar and Kane [28] combined 7 time-frequency transforms of vibration signals from bearings by a convolution neural network. The system was then subjected to deep learning algorithm and optimized for fault classification of the bearings. The method was highly successful and achieved 100% bearing fault classification on all laboratory tests. The authors concluded that their approach would be most suitable for supporting predictive maintenance.

The above literature shows that synchrosqueezed scalogram condition indicator was one of the key indicators contributing to the accurate prediction of faults. The method improves the energy concentration and brings better readability to the scalogram. However, scalogram and synchrosqueezed scalogram methods are good fault indicators when the fault has already happened. When capturing a fault which is still not a fault, synchrosqueezed scalogram is still not sufficient to generate a predictive indicator.

2.4 *Other forms of fault indicators*

System health monitoring methods are normally based on statistical information. Variations of the statistics are required due to characteristics of the application environment. Li et al. [29] utilised massive data recorded in distribution grid to compute linear eigenvalue statistics as a fault indicator. Their method used random matrix theory to derive multiple-dimensional views of the system independent of grid topology and spatiotemporal data. Nguyen et al. [30] surveyed a range of fault indicators specifically designed for stator winding inter-turn faults. The survey compared indicators of different working principles and types. They found that most indicators worked in the fault region, i.e., fault diagnosis, whereas there was a lack of research in the early detection of fault, i.e., fault prognosis. They concluded that a hybrid approach using model-based and sequence component analysis would be necessary to improve health monitoring performance.

Yin and Zhang [31] tried to avoid false fault indicator misreporting by estimating probability of occurrence of fault conditions. The fault indicator was abrupt current lasting for specified time. A mathematical model of fault indicator was simulated and compared with real-time fault indicator signals to determine the fault area more accurately and avoid misinterpretation of the collected information. Likewise, in power quality monitoring, waveform-type disturbance was used as a generic detection indicator [32]. Several abnormality detection methods were investigated. The direct comparison method was found to be most reliable and fast enough for online applications.

Santos and Vieira [33] proposed the concept of fault zone where appropriate health monitoring devices should be installed to capture operating signals. A model of the system was developed to support optimal placement of fault indicators. Li et al. [34] processed massive recorded data in distribution grid using spectral residual algorithm. By combining high-dimension statistical analysis and artificial intelligence methods, they were able to diagnostic accuracy of 98% in real-time.

Location of fault in distribution systems is crucial to rectify faults quickly. Ananthan et al. [35] used fault circuit indicators together with the distribution system model to identify fault sections and subsequently located the fault. However, complex topologies make the locating process difficult. Emerging methods such as interpretable learning models were used to generate parameters that could be monitored for faults by a linear discriminant algorithm enhanced with statistical decision theory and regression analysis [36].

2.5 *Summary of literature review*

Literature review shows that fault indicators vary greatly in different format, data processing and applications. Most fault indicators are fault diagnosis aiming to find out whether there is a fault and where. Very few fault indicators have the ability to detect emerging faults at the early stage of the system's deterioration. There is a research gap that an indicator that can produce recognisable outcomes for early prognosis of the system's health status is required to improve sustainability of system operation.

3. Search for an indicator

Literature review has highlighted the importance of Fourier Transform based digital signal processing methods. In particular, CWT extracts selected sinusoidal signal components into frequency domain where identification of abnormalities seems to be more readily and accurately. With appropriate pattern recognition methodology, the CWT output provides indicators for comparing the state of the system at the time the signal stream is taken. In more pragmatic term, it is indicative of the current state of the system. However, CWT output has one major drawback, i.e., timing information of the signal is lost in domain transformation. Subsequently, the state of the system at the start of the signal stream is indifferent to the state of the system at the end of the signal stream. To monitor the state of the system continuously, large number of signal stream samples are required.

Fortunately, high speed computing and communication platform and Industry 4.0 environment have made continuous data acquisition possible. A new system health condition indicator created from combining synchrosqueezed CWT and scalogram in a new signal segmentation process to compute a serial signal indicator is proposed. The process is illustrated in Figure 1 and explained in the following subsections.

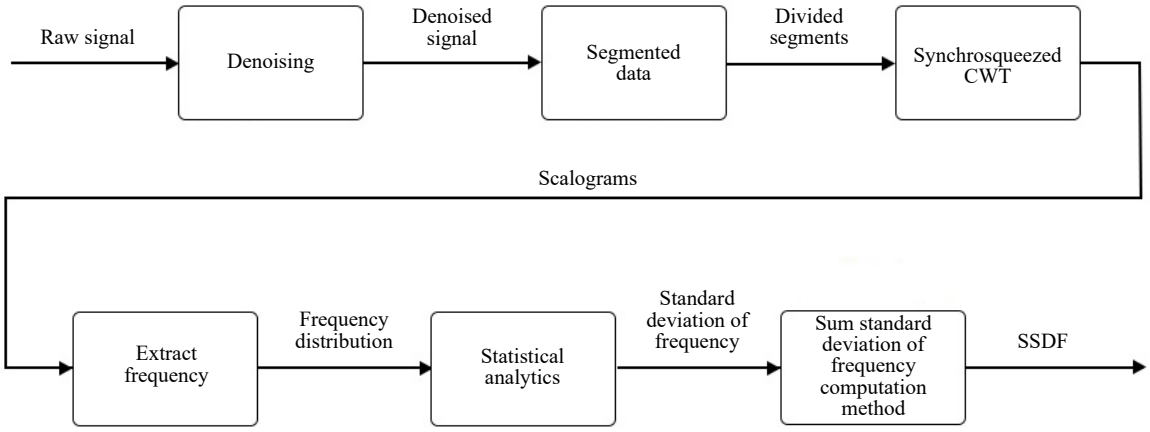

Figure 1. Integrated CWT based trend indicator computation process

3.1 *CWT and scalogram*

During the manufacturing process, signals are obtained in a continuous stream way. These are denoted as "raw signal" in Figure 1. The signal stream is denoted as $x(t)$. Normally, CWT of the raw signal is calculated by Equation (1).

$$W(a,b;\psi) = a^{-\frac{1}{2}} \int_{-\infty}^{\infty} x(t)\overline{\psi_{a,b}(t)}\,dt \tag{1}$$

where $W(a, b; \psi)$ is called CWT coefficient, $\psi_{a,b}(t)$ is a mother wavelet, a is the scale parameter, and b is the shape parameter.

Scalogram of the CWT is the squared absolute value of the coefficient $W_{(a,b;\psi)}$ and can be computed by Equation (2).

$$SG(a,b;\psi) = \left|W(a,b;\psi)\right|^2 \tag{2}$$

However, the traditional way of applying CWT through the whole data stream does not distinguish changes in the signal over time. To retain time-based information during transformation, with the support of Industry 4.0 information technology (IT) capability capturing large number of raw data, the signal stream is segmented.

3.2 *Signal segmentation process*

A new process to split the analysed signal $x(t)$ into segments is proposed. The length of the time segment t_s depends on sampling frequency. Each segment should contain sufficient data points for reasonable CWT analysis. Based on some previous experimentation [37], the standard data set requirement was set at 1,000 data points. To maintain the continuity of the adjacent time segments, an overlap time t_o is set between two adjacent time segments. Length of the time segment and the overlap points can be further adjusted according to the results of initial processing of the CWT signals and its scalogram. Equation (2) is now re-written for all data segments as:

$$SG_i(a,b;\psi) = \left|W_i(a,b;\psi)\right|^2 \tag{3}$$

where i is the number of time segments. If t_T is the total sampled time, the number of time segments is given by:

$$n = \frac{t_T - t_o - 1}{t_S - t_o} \tag{4}$$

Processing of each time segment to an indicator means it is now possible to compute changes of the indicator from one time segment to another. Change of the indicator can then be linked to the time stamp of the segment.

3.3 *Synchrosqueezed wavelet transform and its scalogram*

As discussed in the summary of literature review, CWT scalograms do not have sufficient accuracy of distinguishing abnormal signals. Synchrosqueezed CWT scalogram is introduced to improve the readability of the scalogram. Synchrosqueezed method starts with computing the instantaneous frequency at signal point (a, b) in Equation (5).

$$\omega(a,b) = -j\left[W(a,b)\right]^{-1}\frac{\partial W(a,b)}{\partial b} \tag{5}$$

The synchrosqueezed CWT is then computed by Equation (6).

$$T(\omega_l,b) = \sum\nolimits_{a_k} W(a_k,b)a_k^{-\frac{3}{2}} \tag{6}$$

where a_k satisfies $\left|\omega(a_k,b)-\omega_l\right| \le \Delta\omega/2$.

However, to introduce the ability to distinguish changes over time by raw signal segmentation, the synchrosqueezed method needs to be modified such that the new method should incorporate computation of time segments. Hence, a time segment synchrosqueezed CWT $W_i(a, b)$ will be used instead of $W(a, b; \psi)$ in Equation (7), where i is the number of the time segment.

$$T_{i(\omega_l,b)} = \frac{1}{\Delta\omega}\sum W_i(a_k,b)a_k^{-\frac{3}{2}}\Delta a_k \tag{7}$$

The effect of the modified synchrosqueezed wavelet transform processed by Equation (7) is to transfer CWT coefficient from time domain to time-frequency domain and still hold timing feature in the transformed indicator. The scalogram coefficient $T_i(\omega_l, b)$ can then be computed according to Equation (2).

$$SSG_i(a,b;\psi) = \left|T_i(a,b;\psi)\right|^2 \tag{8}$$

3.4 *Standard deviation of frequency*

The CWT scalogram is effectively a distribution representing frequency components and their strengths (power contained in that frequency). Therefore, it is possible to analyse it statistically, for example, computing its mean and standard deviation. However, CWT scalogram is not clear graphically, which means the statistical properties are not readily distinguishable. Instead, synchrosqueezed CWT scalogram has much better properties for extracting standard deviation of frequency (SDF), F_{stdf} by Equation (9).

$$F_{stdf} = \sqrt{\frac{\sum_1^K (f_k - F_{cf})^2 S_k}{\sum_1^k S_k}} \tag{9}$$

where f_k is the captured special frequency behind extracted features, S_k is the spectrum value, k is the number of lines in a spectrum.

Similarly, S_k is the kth coefficient value of the synchrosqueezed CWT related to the captured special frequency, k is the number of frequencies found in the scalogram. The centre frequency F_{cf} of the scalogram can be computed from Equation (10).

$$F_{cf} = \frac{\sum_1^K f_k S_k}{\sum_1^K S_k} \tag{10}$$

Since the whole-time stream data has been segmented, if there are n time segments, n scalograms will be generated and there are n SDF values in this data set. Graphs are then generated to illustrate the SDF value changes with the time segments.

3.5 *SSDF as condition indicator*

The SDF value changes with time segments in different data sets. It is difficult to observe any singular SDF values from the graph. It changes because of the unstable system conditions causing frequency changes in individual scalogram. To eliminate the instability of SDF, SSDF is proposed. SDF values are the sum of first m SDF in each data set where $m < n$ is the defined number for summing consecutive signal streams, then the SSDF for a data set is given by Equation (11).

$$Z_{stdf} = \sum_{j=1}^{m} F_{jstdf} \tag{11}$$

The first m SDFs are used because this is the period in which mircofaults will start to accumulate but the total effect is still tolerable. Since the synchrosqueezed CWT scalogram is a signal frequency power distribution representing the health condition of the system, the value of SSDF of a data set represents the potential of developing fault within the remaining SDF time frame of the data set. Moreover, computation of SSDF is independent of how the raw signals are acquired making it an ideal indicator that is not affected by the absolute magnitude and original frequency of the raw signals.

4. Experimental setup

To test the proposed theory, a 3D printer was set up as a test bed (Figure 2). The experiment on the printer was conducted under three different scenarios. The first scenario did not contain any fault information, i.e., no fault was introduced in this scenario. In the second and third scenarios, faults were gradually introduced (like a trend of increasing errors). The signals therefore reflected a gradual transfer from normal to abnormal.

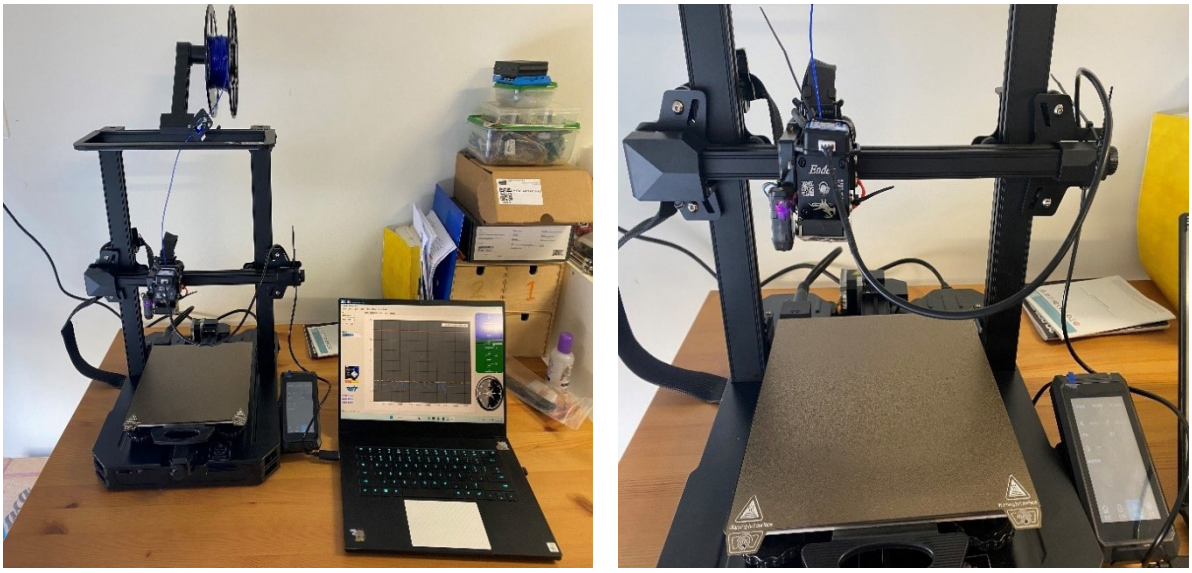

(a) System overview (b) Print head with accelerometer

Figure 2. The 3D printer used for experimental verification

Creality Ender-3 S1 3D printer is used for the experiment. The printer contains two moveable unit, one is the printing platform, another is the printer head which is driven by a timing belt (Figure 3). The tension of the belt can be adjusted by loosening the rotary knob on the printer rack. By slightly loosening the knob in the red circle the tension in the belt can be slightly changed.

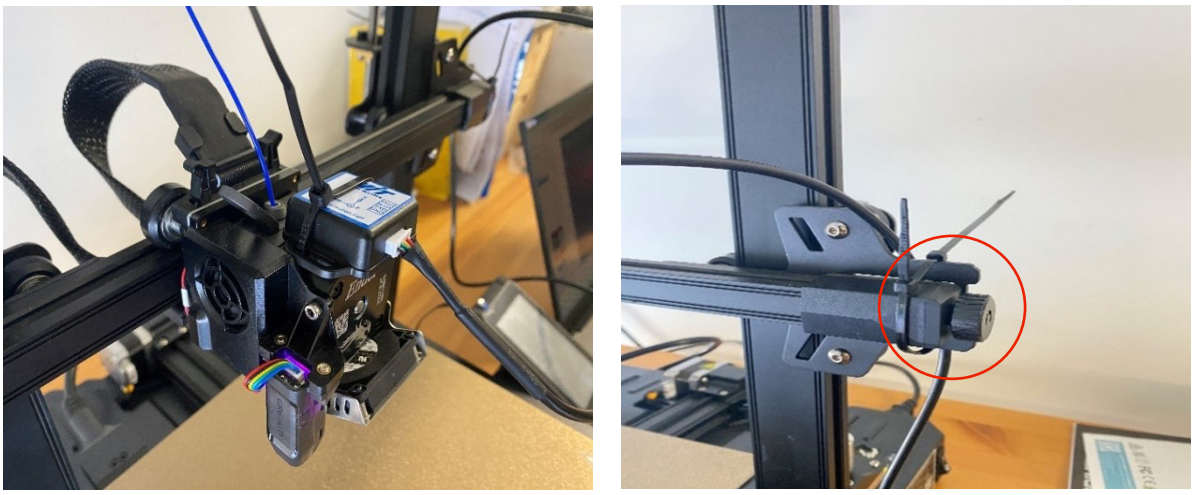

(a) X-axis on the machine (b) The screw that was loosened

Figure 3. The X-axis was tweaked to generate the effect of deteriorating health conditions

Belt tension could influence the movement of the printer head and hence affecting the quality of a workpiece during the printing process. Since the axes were driven by timing belts, small change of belt tension would not immediately induce faults on the workpiece. However, the accumulation of positional inaccuracy would cause some layers of the workpiece being misprinted (Figure 4).

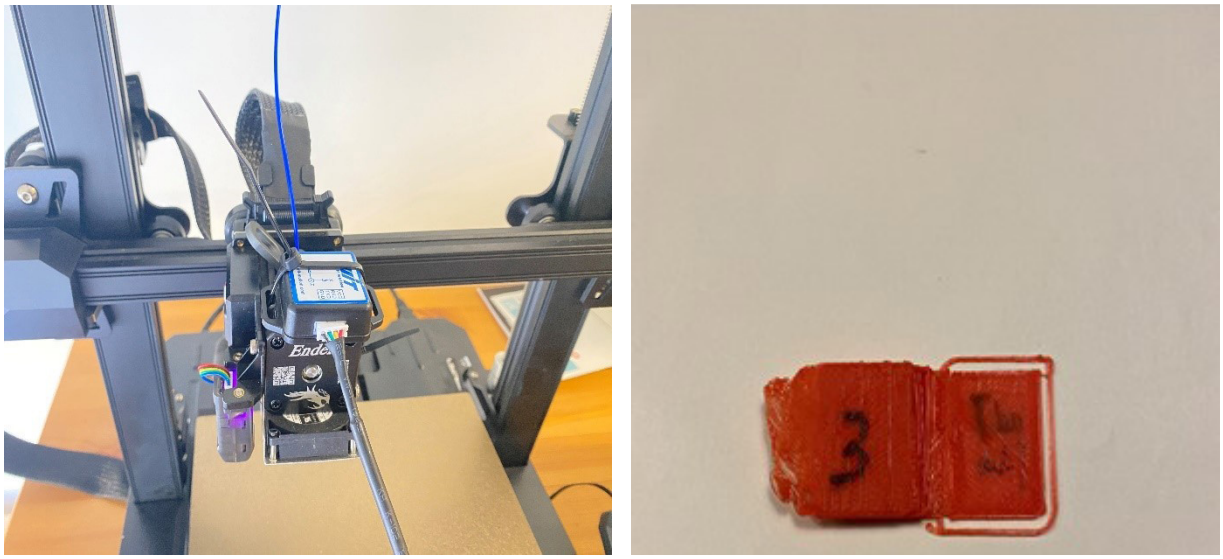

(a) Machine printing while condition deteriorates (b) Discrepancy on workpiece

Figure 4. Small change of belt tension would cause discrepancy on the workpiece

To analyse the belt tension impact on the printer head, an attitude sensor (WT61C232) is attached to the print head. WT61C232 collected acceleration of the printer head in X, Y and Z directions. Data collected by the sensor was transferred to the laptop through a direct connection cable.

A rectangle block was iteratively printed under different scenarios. Three types of experiments were conducted. The time to print one block was 15.5 minutes.

In the first type of experiments, a block was printed at normal conditions. These blocks were collected as quality benchmarks. For easier reference in Section 5, this type of experiments was recorded as “normal” operation. 43 experiments were run in “normal” mode.

In the second type of experiments, the first 6 minutes were “normal” runs. The machine maintained the same tension as the first type of experiments. Starting from 7th minute, the screw was loosened at a constant speed of one minute per revolution. This process repeated until 6 revolutions were completed. No further loosening was done, and the printer continued to 3D print the workpiece until complete. The reason to stop at 6th revolution was that the 3D printing condition was still acceptable. There was minor misalignment of layers, but the effect was hardly measurable. Therefore, the second type of experiments was recorded as “marginal” operation meaning that the outcomes were acceptable. 37 experiments were run in “marginal” mode.

In the third type of experiments, the first 12 minutes were the same as in the second type of experiments. Starting from 13th minute, instead of stopping to loosen, the belt was further loosened by two resolutions. Faults started to display on the block. Surface of the block was damaged. Since the 3D printing process failed, this type of experiments was recorded as “abnormal” operation. 20 experiments were run in “abnormal” mode.

5. Results and analysis

Acceleration data of the axes were logged by the WT61C232 attitude sensor. It took 15.5 minutes to print one rectangular block. Since the first 6 minutes of every print were set at the machine’s original condition, i.e., as a well-maintained normal machine, focus on analysis is on raw signals from 6 to 14 minutes. Sampling frequency was 100 Hz which gave 100 signal points per second, or total 48,000 signal points per data set. The 48,000 signal points were cut into segments of 1,000 points each (with overlap). The following sections explain the computational process of SSDF.

5.1 *Step 1. Denoise the raw signal*

Different denoising methods have been tried to remove the noise out of the signal. The denoised outcomes of wavelet packet transform (WPT) [38], empirical mode decomposition (EMD) [39], and average filtering are displayed in Figure 5.

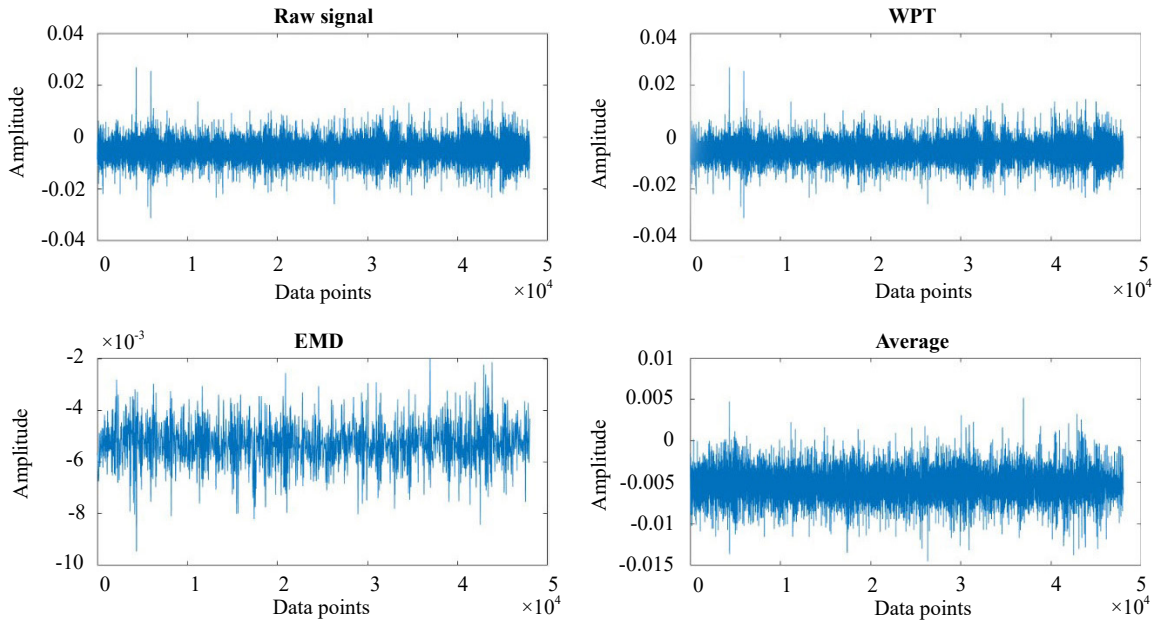

Figure 5. Outcome of different signal denoising methods applied to the raw signal

These methods are not effective. Instead, the ensemble empirical mode decomposition (EEMD) [40] shows promising results (Figure 6).

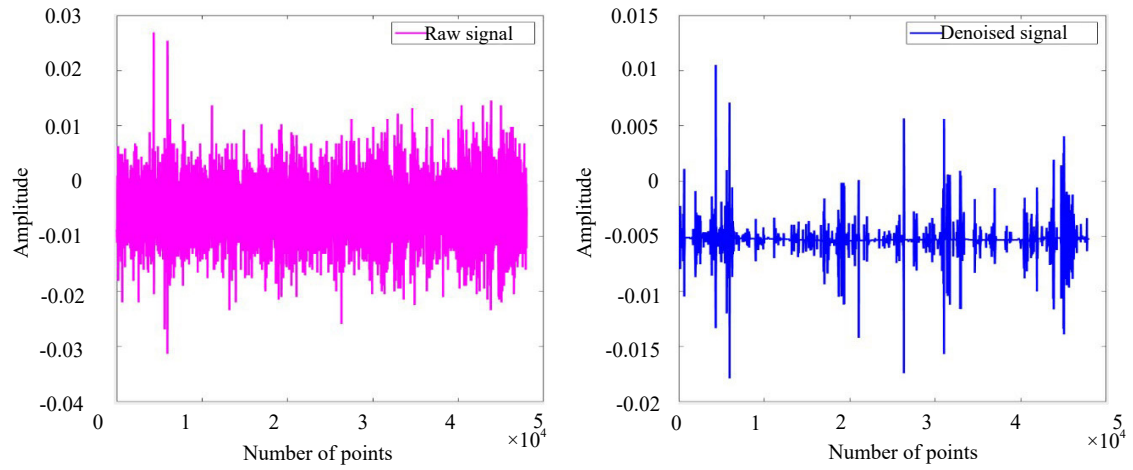

Figure 6. EEMD denoised results

5.2 *Step 2. Data segments*

As explained in Section 3.2, overlap points are added to the segmented data stream to a void missing information and keep the continuity between adjacent time segments. After some trials, 10 seconds per time segment (1,000 points/segment) with 3 second overlap time shows the best results in the experiment. By applying Equation (4), $n = \frac{t_T - t_o - 1}{t_s - t_o} = \frac{480 - 3 - 1}{10 - 3} = 68$. This means 68 synchrosqueezed transformed signal segments were used to generate the corresponding scalograms.

5.3 *Step 3. Synchrosqueezed scalogram*

Figure 7 compares a CWT scalogram with a synchrosqueezed CWT scalogram. The X-axis is the data points in 10 seconds. Y-axis is the frequency information during the CWT transform. It can be observed that synchrosqueezed CWT scalogram distinguishes frequency concentration more clearly than the CWT scalogram. Hence, all data sets were converted by synchrosqueezed CWT to form scalograms according to the mathematical treatment explained in Section 3.3.

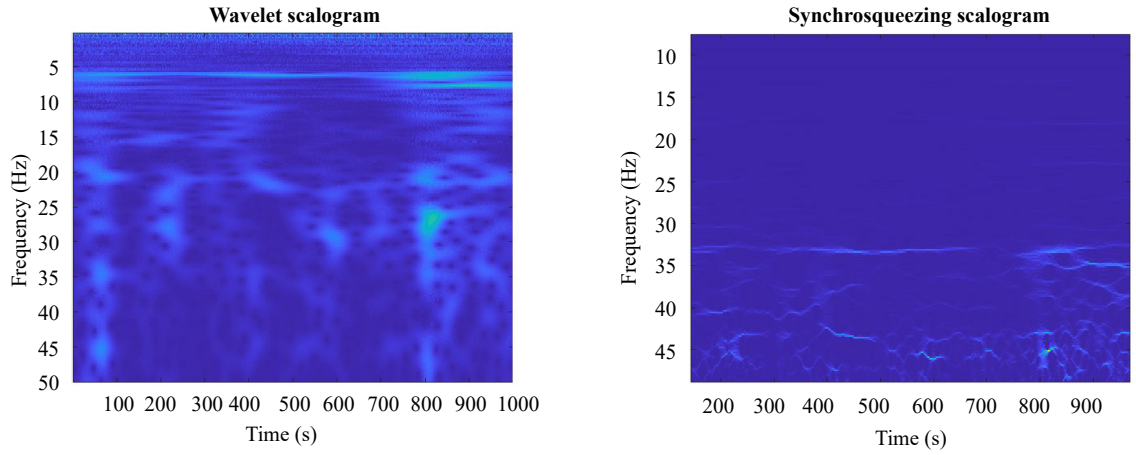

Figure 7. Comparison of outcomes between CWT and synchrosqueezed CWT scalograms

5.4 *Step 4. Compute SDF*

The synchrosqueezed CWT scalograms were processed according to SDF values according to the theory in Section 3.4. Figure 8 shows the SDF value changes of four data sets in “normal” experiments. The X-axis is the time segment (expressed in seconds). The Y-axis is the SDF values. There was no fault in this “normal” situation. In the 43 data sets, it was found that most high SDF values appeared in the first 20 time segments. The remaining SDF values were relatively flat. Based on this observation, the value of m in Equation (11) is set at 20.

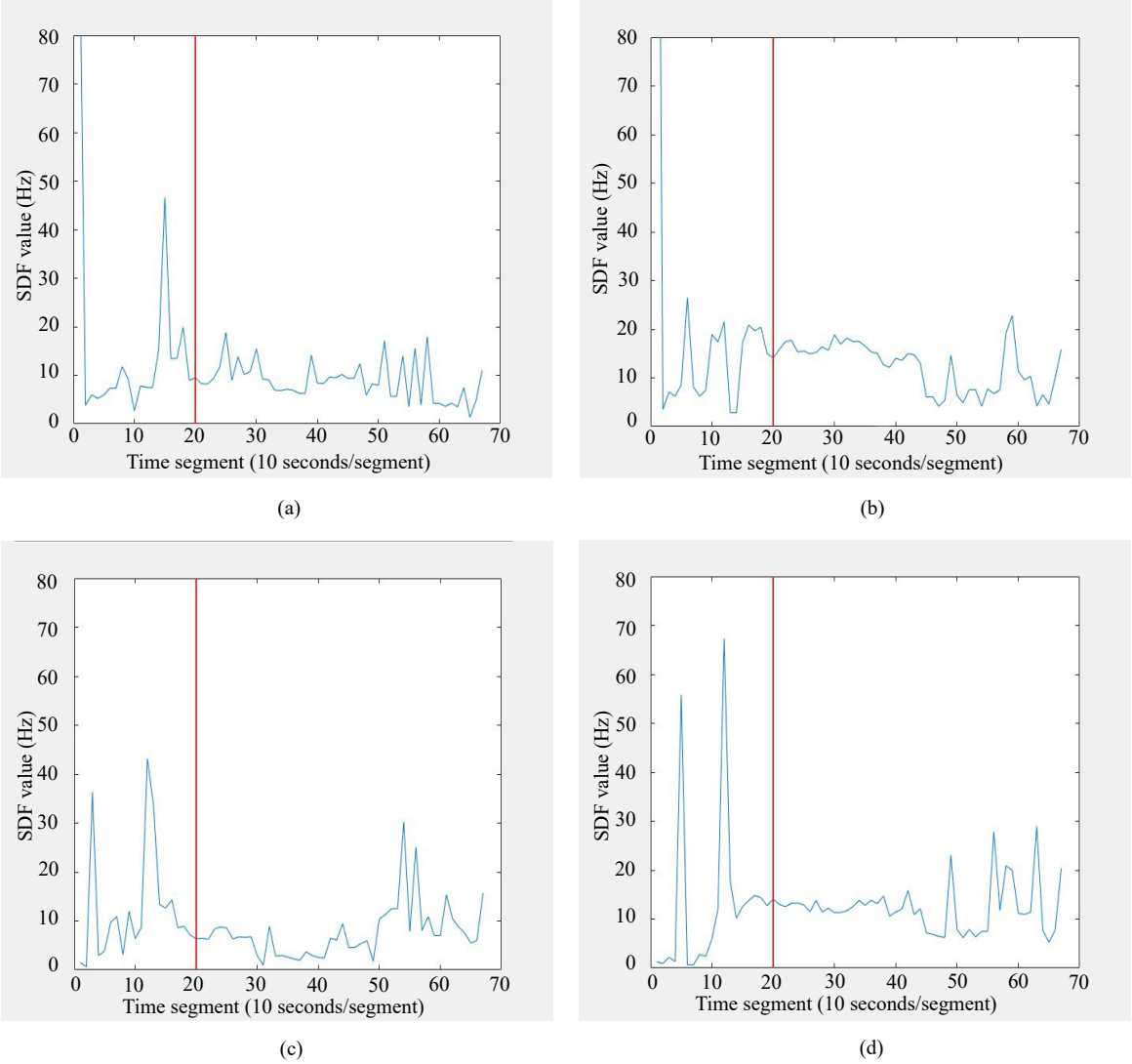

Figure 8. SDF values in time segments for "normal" experiments

Figure 9 shows the SDF values in "marginal experiments, in which the first 6 minutes were "normal" operation and the belt tension was loosened from 7th minute for 6 minutes then stopped. The quality of the workpiece was still acceptable. Figure 9 shows that the SDF value changes for 4 typical "marginal" runs. Large SDF values are still common in the first 20 time segments but they are not as obvious as the "normal" experiments.

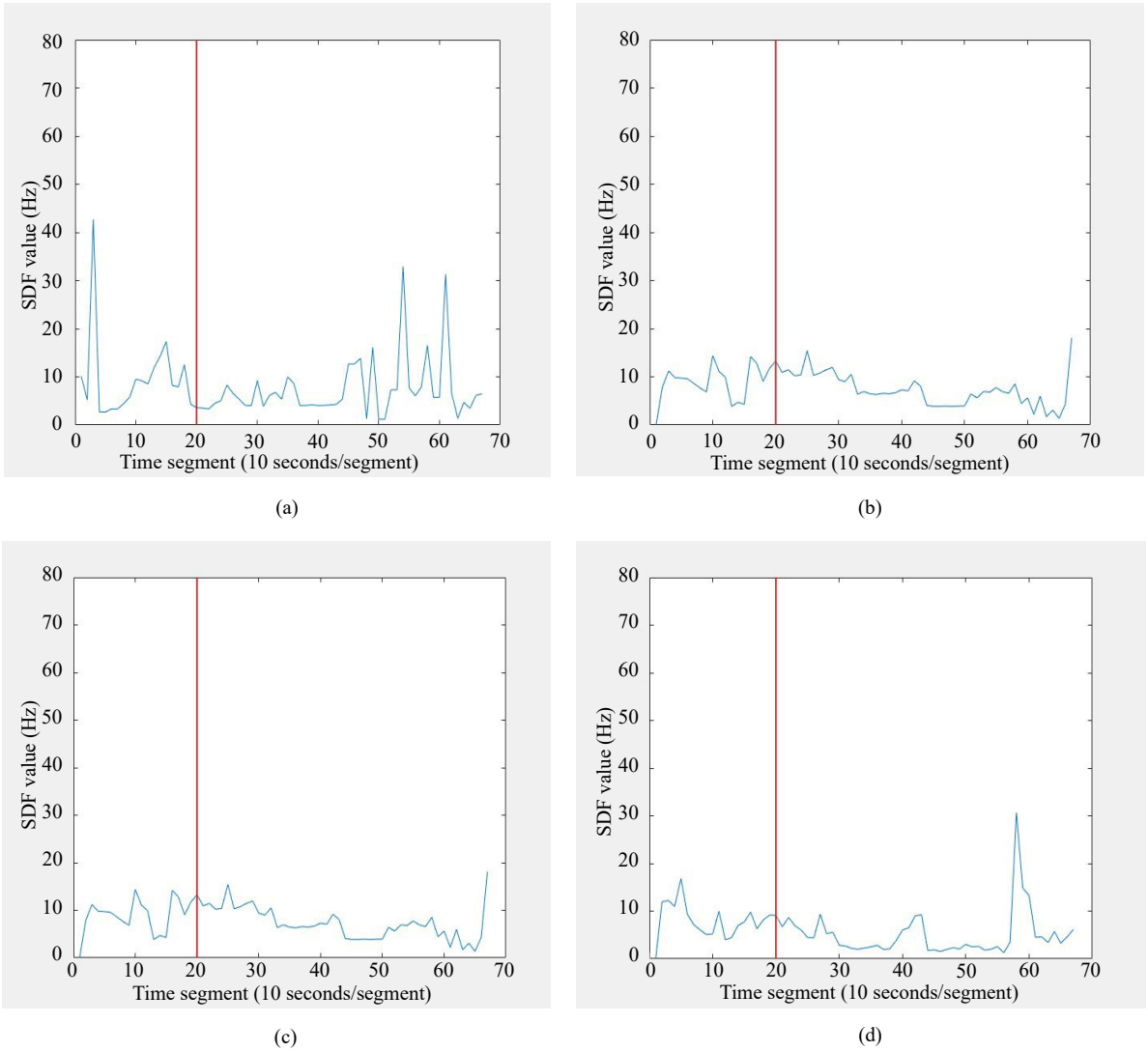

Figure 9. SDF values in time segments for "marginal" experiments

Figure 10 shows the SDF value from data collected in "abnormal" experiments. The belt was loosened to such an extent that machine movements were affected seriously. Quality of the workpiece was not acceptable or actually misprinted. In Figure 10, four typical "abnormal" runs are displayed. Some occasional spikes are observed but the overall SDF value variation is flat.

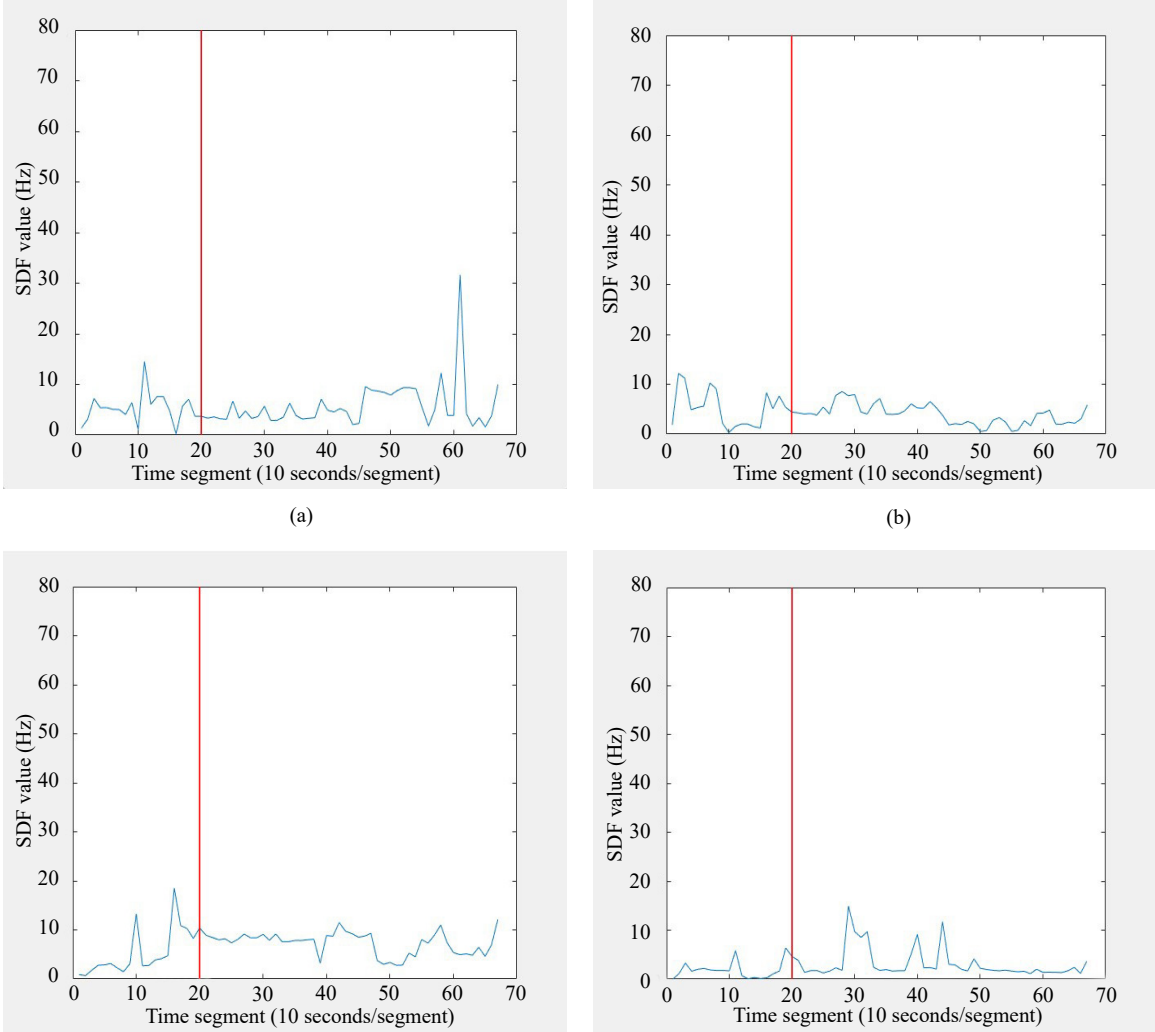

Figure 10. SDF values in time segments for "abnormal" experiments

5.5 *Step 5. SSDF value changes with time segments*

Instead of observing the single SDF value changes with data set, finding a value which can distinguish the experiment type clearly is the goal of this research. Having acquired the data, and due to observation in Section 5.4, m is set at 20. Therefore, the first 20 SDF values are added together in each data set and created a parameter called SSDF, as explained in Section 3.5.

Figure 11 shows the combined histogram of SSDF values for all three types of experiments. The X-axis is intervals of SSDF values. The interval width is 10, i.e., if the mid-point of the interval SSDF $S = 105$, then the range of SSDF is:

$$100 \leq S < 110 \tag{12}$$

Intervals with mid-points from 5, 15, 25, …, 335 are plotted in Figure 11.

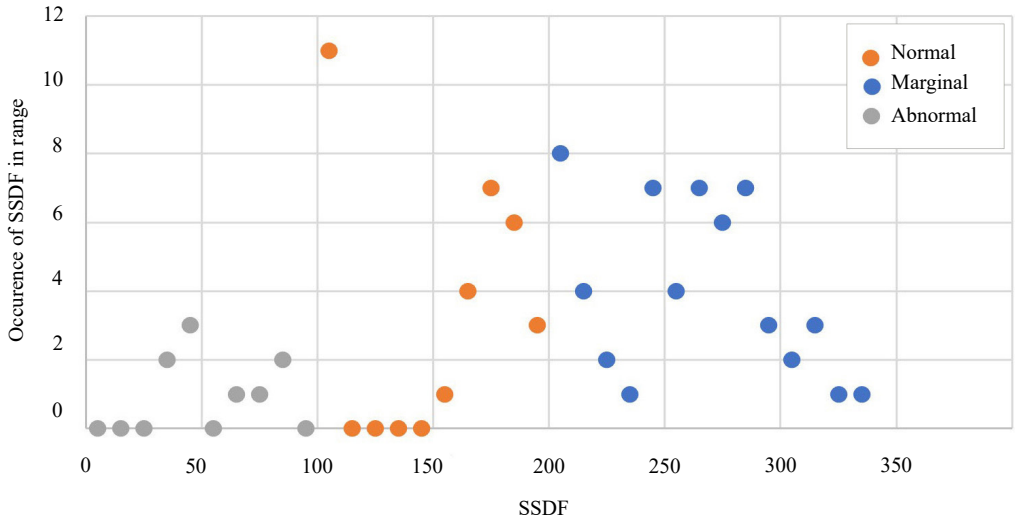

Figure 11. SSDF histogram for normal, marginal and abnormal experiments

It is clear from Figure 11 that normal operations gave the highest SSDF values between 250 to 350. Marginal operations gave SSDF values between 150 to 250. Abnormal operations gave SSDF values below 150.

As the process is continuously monitored, decreasing SSDF values will indicate condition deteriorating. Actions should be taken when the system is still marginal to avoid producing rejects when it turns into abnormal state.

6. Discussion

SSDF indicator originates from SDF. A primary question of concern is how significant SDF as an indicator of machine condition can be compared to other indicators such as entropy [41], standardised indicator [42], Kurtosis [43]. Three weight evaluation methods have been used to evaluate the influence of these indicators on decision making.

The entropy weight method is a branch of information theory. It can capture the implied interactions among features and be commonly used to measure value dispersion in decision-making [44]. Relief F method is a distance-based feature selection algorithm exclusively for classification problems with two classes, whose core idea is to assign different weights denoting importance to attributes according to their values that distinguish between instances near to each other [45]. The principal component analysis (PCA) method is a multivariate data analysis methods [46]. The mean goal of PCA is to achieve dimensionality reduction with the minimum mean square error [47].

Using these three weight evaluation methods, the weights for the four indicators are computed as shown in Table 1.

Table 1. Weight of different indicators according to weight methods

Weight method	SDF	Entropy	Standardised indicator	Kurtosis
Entropy weight	0.2534	0.4091	0.1454	0.1921
Relief F	0.0625	0.0586	5.5758×10^{-4}	0.0822
PCA	56.8005	-19.8564	-24.8591	-12.0850

For the entropy weight method, the lower the entropy is, the more information an indicator provides, and the higher

the weight of that indicator. From Table 1, entropy of the data set has the largest weight value which contains redundant information. SDF has the second largest value, and standardised indicator has the smallest value.

For the Relief F method, Kurtosis has the highest average weight value, SDF and entropy have almost the same average weight.

For the PCA method, although the weight of different indicators is not identical, standardised indicator has the lowest value and is considered not influential. On the other hand, SDF and entropy are close to each other. The entropy weight method shows entropy has more weight, but the Relief F method shows SDF is more critical. Therefore, it can be concluded from the above evaluation that SDF is one of the top indicators.

7. Conclusion

Fault indicators in system diagnosis are good to identify faults when they occur but that is too late to prevent machine malfunction and rejects. System health indicators in literature are often computed and applicable to specific application context and may not be useful for other systems. In this paper, a new system health condition indicator SSDF has been proposed and demonstrated in experiments. The main contribution of this research is that a new numerical indicator that is independent of the application context and is able to trigger warning to fault condition when the system is still at acceptable operating condition is defined and validated.

The theoretical foundation of SSDF originates from a novel time segmentation process that divides raw signal streams to time significance segmented data streams. Each of the segmented data streams is analysed by synchrosqueezed CWT and their corresponding scalograms are computed.

The SDF values computed in each time segment are good indicators of the state of the process. Synchrosqueezed CWT zooms into the part of frequency spectrum where major portion of signal power is. Instead of measuring the power directly from the scalograms, SDF can be computed from the distribution of frequency of each time segment. By adding first 20 SDFs in each of the data sets, the new trend indicator, SSDF, shows changes of system conditions in a form that is independent from where the original signal comes from. Histogram of SSDF shows clearly that there are distinct regions of SSDF values for “normal”, “marginal” and “abnormal” operations.

Since SSDF relies on feeding raw signal data, so long as sufficient data points are available, the steps described in this paper to compute SSDF indicator can be done continuously thereby achieving the goal of continuous system health monitoring. The nature of continuous health monitoring requires large amount of raw data to be collected and is particularly suitable for new industry environment such as Industry 4.0 where system sensors and data communication capabilities are well established.

Conflict of interest

There is no conflict of interest for this study.

References

[1] Setiawan A, Angela D, Irawan B. Modelling of cutting tool condition monitoring system (CTCMS) to support Industry 4.0. *International Mechanical and Industrial Engineering Conference 2018 (IMIEC 2018)*. 2018; 204: 02012. https://doi.org/10.1051/matecconf/201820402012

[2] German-Sallo Z, Strnad G. Machinery fault diagnosis using signal analysis. *Procedia Manufacturing*. 2019; 32: 585-590. https://doi.org/10.1016/j.promfg.2019.02.256

[3] Wei S, Zhao H, Jing J, Liu Y. Investigation on surface micro-crack evaluation of engineering ceramics by rotary ultrasonic grinding machining. *The International Journal of Advanced Manufacturing Technology*. 2015; 81: 483-492. https://doi.org/10.1007/s00170-015-7195-y

[4] Long J, Wang X, Zhou W, Zhang J, Dai D, Zhu G. A comprehensive review of signal processing and machine learning technologies for UHF PD detection and diagnosis (I): Preprocessing and localization approaches. *IEEE*

Access. 2021; 9: 69876-69904. https://doi.org/10.1109/ACCESS.2021.3077483

[5] Kia SH, Henao H, Capolino GA. Digital signal processing for induction machines diagnosis - A review. In: *IECON 2007 - 33rd Annual Conference of the IEEE Industrial Electronics Society*. Taipei, Taiwan: IEEE; 2007. p.1155-1162. https://doi.org/10.1109/IECON.2007.4460325

[6] Xu H, Ma R, Yan L, Ma Z. Two-stage prediction of machinery fault trend based on deep learning for time series analysis. *Digital Signal Processing*. 2021; 117: 103150. https://doi.org/10.1016/j.dsp.2021.103150

[7] Qiu X, Du X. Fault diagnosis of TE process using LSTM-RNN neural network and BP Model. In: *2021 IEEE 3rd International Conference on Civil Aviation Safety and Information Technology (ICCASIT)*. Changsha, China: IEEE; 2021. p.670-673. https://doi.org/10.1109/ICCASIT53235.2021.9633621

[8] Pedrosa VD, Vieira JCM. Fault location using modern fault indicators in the presence of distributed generation. In: *2018 Simposio Brasileiro de Sistemas Eletricos (SBSE)*. Niteroi, Brazil: IEEE; 2018. p.1-6. https://doi.org/10.1109/SBSE.2018.8395733

[9] Zhao Q, Gao H, Yuan T, Li L, Wang G. Fault indicator three-phase synchronization method based on fault instant. In: *2022 IEEE/IAS Industrial and Commercial Power System Asia (I&CPS Asia).* Shanghai, China: IEEE; 2022. p.275-281. https://doi.org/10.1109/ICPSAsia55496.2022.9949961

[10] El-Shafie A, Noureldin A, McGaughey D, Hussain A. Fast orthogonal search (FOS) versus fast Fourier transform (FFT) as spectral model estimations techniques applied for structural health monitoring (SHM). *Structural and Multidisciplinary Optimization*. 2012; 45: 503-513. https://doi.org/10.1007/s00158-011-0695-y

[11] Yang L, Sheu SH. Integrating multivariate engineering process control and multivariate statistical process control. *The International Journal of Advanced Manufacturing Technology*. 2006; 29: 129-136. https://doi.org/10.1007/s00170-004-2494-8

[12] Yang SYS, Kearney T, Mo JPT, Boland P. MachineGP: a new concept in signal-based machine condition monitoring and diagnostics. *New Engineer Journal*. 2003; 7(2): 19-23. http://hdl.handle.net/102.100.100/190772?index=1

[13] Balamurugan R, Al-Janahi F, Bouhali O, Shukri S, Abdulmawjood K, Balog RS. Fourier Transform and Short-Time Fourier Transform decomposition for photovoltaic arc fault detection. In: *2020 47th IEEE Photovoltaic Specialists Conference (PVSC)*. Calgary, AB, Canada: IEEE; 2020. p.2737-2742. https://doi.org/10.1109/PVSC45281.2020.9300455

[14] Ahmadi HR, Mahdavi N, Bayat M. A novel damage identification method based on short time Fourier transform and a new efficient index. *Structures*. 2021; 33: 3605-3614. https://doi.org/10.1016/j.istruc.2021.06.081

[15] Peng ZK, Chu FL. Application of the wavelet transform in machine condition monitoring and fault diagnostics: a review with bibliography. *Mechanical Systems and Signal Processing*. 2004; 18(2): 199-221. https://doi.org/10.1016/S0888-3270(03)00075-X

[16] Manarikkal I, Elasha F, Mba D. Diagnostics and prognostics of planetary gearbox using CWT, auto regression (AR) and K-means algorithm. *Applied Acoustics*. 2021; 184: 108314. https://doi.org/10.1016/j.apacoust.2021.108314

[17] Lapins S, Roman DC, Rougier J, De Angelis S, Cashman KV, Kendall JM. An examination of the continuous wavelet transform for volcano-seismic spectral analysis. *Journal of Volcanology and Geothermal Research*. 2020; 389: 106728. https://doi.org/10.1016/j.jvolgeores.2019.106728

[18] Lee SH, Lim JS, Kim JK, Yang J, Lee Y. Classification of normal and epileptic seizure EEG signals using wavelet transform, phase-space reconstruction, and Euclidean distance. *Computer Methods and Programs in Biomedicine*. 2014; 116(1): 10-25. https://doi.org/10.1016/j.cmpb.2014.04.012

[19] Narin A. Detection of focal and non-focal epileptic seizure using continuous wavelet transform-based scalogram images and pre-trained deep neural networks. *IRBM*. 2022; 43(1): 22-31. https://doi.org/10.1016/j.irbm.2020.11.002

[20] Feng S, Mo JP. Efficacy study of fault trending algorithm to prevent fault occurrence on automatic trampoline webbing machine. *Applied Sciences*. 2022; 12(3): 1708. https://doi.org/10.3390/app12031708

[21] Silva A, Zarzo A, González JM, Munoz-Guijosa JM. Early fault detection of single-point rub in gas turbines with accelerometers on the casing based on continuous wavelet transform. *Journal of Sound and Vibration*. 2020; 487: 115628. https://doi.org/10.1016/j.jsv.2020.115628

[22] Yesilyurt I. The application of the conditional moments analysis to gearbox fault detection—a comparative study using the spectrogram and scalogram. *NDT & E International*. 2004; 37(4): 309-320. https://doi.org/10.1016/j.ndteint.2003.10.005

[23] Ozturk H, Sabuncu M, Yesilyurt I. Early detection of pitting damage in gears using mean frequency of scalogram. *Journal of Vibration and Control*. 2008; 14(4): 469-484. https://doi.org/10.1177/1077546307080026
[24] Wu YH, Zhang DZ, Li XL, Xue JF. Research on aeroengine rub-impact fault analysis based on wavelet scalogram statistical feature. *Applied Mechanics and Materials*. 2011; 48-49: 942-945. https://doi.org/10.1109/ICWAPR.2010.5576414
[25] Daubechies I, Lu J, Wu HT. Synchrosqueezed wavelet transforms: An empirical mode decomposition-like tool. *Applied and Computational Harmonic Analysis*. 2011; 30(2): 243-261. https://doi.org/10.1016/j.acha.2010.08.002
[26] Thakur G, Brevdo E, Fučkar NS, Wu HT. The synchrosqueezing algorithm for time-varying spectral analysis: Robustness properties and new paleoclimate applications. *Signal Processing*. 2013; 93(5): 1079-1094. https://doi.org/10.1016/j.sigpro.2012.11.029
[27] Mihalec M, Slavic J, Boltezar M. Synchrosqueezed wavelet transform for damping identification. *Mechanical Systems and Signal Processing*. 2016; 80: 324-334. https://doi.org/10.1016/j.ymssp.2016.05.005
[28] Gundewar SK, Kane PV. Bearing fault diagnosis using time segmented Fourier synchrosqueezed transform images and convolution neural network. *Measurement*. 2022; 203: 111855. https://doi.org/10.1016/j.measurement.2022.111855
[29] Li F, He X, Chen R, Wu Y, Tian Y. Distribution grid fault diagnosis based on fault indicator and random matrix. *Journal of Physics: Conference Series*. 2023; 2425: 012001. https://doi.org/10.1088/1742-6596/2425/1/012001
[30] Nguyen VH, Wang D, Yu M, Vaiyapuri V, Nadarajan S. A survey of fault indicators for stator winding inter-turn fault detection in low-voltage induction machines. In: *2015 IEEE 10th Conference on Industrial Electronics and Applications (ICIEA)*. Auckland, New Zealand: IEEE; 2015. p.1380-1385. https://doi.org/10.1109/ICIEA.2015.7334324
[31] Yin Z, Zhang W. Fault diagnosis method of fault indicator based on maximum probability. *IOP Conference Series: Materials Science and Engineering*. 2017; 199: 012068. https://doi.org/10.1088/1757-899X/199/1/012068
[32] Luo J, Yan R, Saha T, Sharma R. Waveform abnormality detection method for distribution system equipment condition monitoring. *International Journal of Electrical Power & Energy Systems*. 2023; 152: 109267. https://doi.org/10.1016/j.ijepes.2023.109267
[33] Santos GG, Vieira JCM. Optimal placement of fault indicators to identify fault zones in distribution systems. *IEEE Transactions on Power Delivery*. 2021; 36(5): 3282-3285. https://doi.org/10.1109/TPWRD.2021.3101671
[34] Li F, He X, Chen R, Wu Y, Tian Y. Distribution grid fault diagnosis based on SR-GRU and fault indicator. In: *2022 International Conference on Computer Engineering and Artificial Intelligence (ICCEAI)*. Shijiazhuang, China: IEEE; 2022. p.857-861. https://doi.org/10.1109/ICCEAI55464.2022.00179
[35] Ananthan SN, Bastos AF, Santoso S, Chirapongsananurak P. Model-based approach integrated with fault circuit indicators for fault location in distribution systems. In: *2019 IEEE Power & Energy Society General Meeting (PESGM)*. Atlanta, USA: IEEE; 2019. https://doi.org/10.1109/PESGM40551.2019.8973516
[36] Chen Y, Wang D, Hou B, Xia T. Gaussian assumptions-free interpretable linear discriminant analysis for locating informative frequency bands for machine condition monitoring. *Mechanical Systems and Signal Processing*. 2023; 199: 110492. https://doi.org/10.1016/j.ymssp.2023.110492
[37] Feng S, Mo JPT. Fault trending of an automatic double threaded trampoline webbing machine. In: *2020 11th International Conference on Prognostics and System Health Management (PHM-2020 Jinan)*. Jinan, China: IEEE; 2020. p.281-285. https://doi.org/10.1109/PHM-Jinan48558.2020.00056
[38] Plaza EG, Lopez PJN. Application of the wavelet packet transform to vibration signals for surface roughness monitoring in CNC turning operations. *Mechanical Systems and Signal Processing*. 2018; 98: 902-919. https://doi.org/10.1016/j.ymssp.2017.05.028
[39] Kumar S, Panigrahy D, Sahu PK. Denoising of Electrocardiogram (EGG) signal by using empirical mode decomposition (EMD) with non-local mean (NLM) technique. *Biocybernetics and Biomedical Engineering*. 2018; 38(2): 297-312. https://doi.org/10.1016/j.bbe.2018.01.005
[40] Wu ZH, Huang NE. Ensemble empirical mode decomposition: A noise-assisted data analysis method. *Advances in Adaptive Data Analysis*. 2009; 1(1): 1-41. https://doi.org/10.1142/S1793536909000047
[41] Li X, Dai K, Wang Z, Han W. Lithium-ion batteries fault diagnostic for electric vehicles using sample entropy analysis method. *Journal of Energy Storage*. 2020; 27: 101121. https://doi.org/10.1016/j.est.2019.101121

[42] Wei Z, Wang Y, He S, Bao J. A novel intelligent method for bearing fault diagnosis based on affinity propagation clustering and adaptive feature selection. *Knowledge-Based Systems*. 2017; 116: 1-12. https://doi.org/10.1016/j.knosys.2016.10.022

[43] Chen B, Shen B, Chen F, Tian H, Xiao W, Zhang F, et al. Fault diagnosis method based on integration of RSSD and wavelet transform to rolling bearing. *Measurement*. 2019; 131: 400-411. https://doi.org/10.1016/j.measurement.2018.07.043

[44] Li Z, Luo Z, Wang Y, Fan G, Zhang J. Suitability evaluation system for the shallow geothermal energy implementation in region by Entropy Weight Method and TOPSIS method. *Renewable Energy*. 2022; 184: 564-576. https://doi.org/10.1016/j.renene.2021.11.112

[45] Dou J, Song Y, Wei G, Zhang Y. Fuzzy information decomposition incorporated and weighted Relief-F feature selection: When imbalanced data meet incompletion. *Information Sciences*. 2022; 584: 417-432. https://doi.org/10.1016/j.ins.2021.10.057

[46] Sadek O, Touhtouh S, Bouabdalli EM, Hajjaji A. Development of a protocol for the rapid identification of solid materials using the principal component analysis (ACP) method: Case of phosphate fertilizers. *Materials Today: Proceedings*. 2022; 66(1): 402-407. https://doi.org/10.1016/j.matpr.2022.06.083

[47] Li P, Zhang W, Lu C, Zhang R, Li X. Robust kernel principal component analysis with optimal mean. *Neural Networks*. 2022; 152: 347-352. https://doi.org/10.1016/j.neunet.2022.05.005